INSTITUTE OF PHYSICS PUBLISHING JOURNAL OF MICROMECHANICS AND MICROENGINEERING

J. Micromech. Microeng. **14** (2004) 1190–1196 PII: S0960-1317(04)76172-0

Macromodeling of coupled-domain MEMS devices with electrostatic and electrothermal effects*

Yao-Joe Yang, Szu-Yuan Cheng and Kuo-Yeh Shen

Department of Mechanical Engineering, National Taiwan University, Taipei, Taiwan, ROC

Received 16 February 2004
Published 17 June 2004
Online at stacks.iop.org/JMM/14/1190
doi:10.1088/0960-1317/14/8/011

Abstract

In this paper, a macromodeling procedure for coupled-domain MEMS devices with electrostatic and electrothermal effects is presented. Transient fully-meshed simulations using finite-element or finite-difference methods (FEM/FDM) for coupled-domain systems require tremendous computational cost. Therefore, in this work, we use the Karhunen-Loeve/Galerkin technique for extracting the macromodels that capture the system's nonlinear behaviors, such as the structural dynamics, the squeeze-film damping and the electrostatic actuation. In addition, using the Arnoldi-based technique, the thermal macromodels are reduced from the linear FEM/FDM models. The system dynamic behavior is successfully reproduced by using these macromodels. Compared with the fully-meshed model, the computational cost of the macromodels is reduced by at least a factor of 500 with less than 1% error. Experimental verifications for the simulated results are also provided.

(Some figures in this article are in colour only in the electronic version)

1. Introduction

System-level simulations of MEMS devices are essential for dynamic performance prediction and optimization. One of the key requirements for such simulations is the development of efficient and accurate macromodels that are compatible with system-level solvers [1]. The most typical way of creating macromodels is to use the lumped-element approach. Although the macromodel created by this approach is intrinsically compatible with any circuit simulators, many costly FEM/FDM simulations may be required for extracting appropriate lumped elements. Furthermore, the accuracy of the lumped-element approach is detrimentally affected if either the original device geometry is too complicated or the coupled-domain dynamical behavior is highly nonlinear. Therefore, various techniques for extracting MEMS macromodels have been proposed. For linear or weakly nonlinear systems, the macromodels can be easily obtained by reducing the finite-element (FEM) or finite-difference (FDM) formulations using the Arnoldi or the quadratic techniques [2–5]. These approaches are very efficient and accurate for linear systems with complicated geometries, but are incapable of capturing the dynamical behavior for nonlinear systems over a wide range of operating conditions. Rewienski, *et al* [6, 7] proposed an algorithm which piecewise-linearly integrates the linear compact models generated by the Arnoldi method at different operating points. This algorithm intelligently evaluates the weighting of each linear macromodel based on the error between the training trajectory and the actual operating trajectory. If the actual operating trajectory is close to the training trajectory, this algorithm has been demonstrated to be efficient and accurate for highly nonlinear systems.

The reduced-order models generated by the Karhunen-Loeve/Galerkin approach [8–10], on the other hand, are based on the basis functions extracted from an ensemble of the snapshots of the physical fields (e.g., pressure distribution or temperature distribution) under certain actuation conditions, and have been proved to be very efficient and accurate for macromodeling nonlinear systems. However, this approach requires expensive coupled-domain FEM/FDM runs to provide enough snapshot data for extracting basis

* This paper is an extension of the paper that was orally presented at Transducers '03 (Paper ID:3A3.5).

functions. Furthermore, as will be discussed in this paper, the efforts required for implementing and simulating the FEM/FDM runs increase exponentially if any new physical domain is introduced into the system.

In this work, we extend the nonlinear macromodeling work presented in [9] by combining the Karhunen-Loeve/Galerkin and the Arnoldi methods for efficient macromodeling of very complex coupled-domain systems. For nonlinear domains, such as structural dynamics and fluidic damping effect, the Karhunen-Loeve/Galerkin method is used. For linear domains, such as the electrothermal effect, the Arnoldi algorithm is applied to generate the reduced-order models. A MEMS example, which includes structural mechanics, squeeze-film damping effect, electrostatics and electrothermal effects, will be introduced and studied using the techniques presented in this work.

2. Karhunen-Loeve decomposition for basis functions

In this section, we briefly describe the fundamentals of using the Karhunen-Loeve (K-L) decomposition technique to extract the basis functions for nonlinear coupled-domain MEMS systems. The K-L decomposition technique was originally developed for representing a stochastic field with a minimum degree of freedom [10]. This method is desirable for coupled-domain MEMS dynamical modeling because it yields a small set of orthogonal basis functions that are capable of representing the physical field distributions of nonlinear systems when used with the Galerkin method. In this work, the K-L decomposition is applied to extract the basis functions from a snapshot ensemble of physical fields obtained from transient coupled-domain FEM/FDM simulations. The brief description is as follows.

Given N temporal snapshots of field distributions v_n, where $n = 1, 2, \ldots, N$, the process of extracting the first few basis functions, denoted by φ, which capture the characteristics of the v_n best, is equivalent to maximizing λ, which is defined in equation (1), for each corresponding basis function φ.

$$\lambda = \frac{\langle(\varphi, v_n)^2\rangle}{(\varphi, \varphi)}. \tag{1}$$

Here we define the inner product of two functions f and g in the function space Ω as $(f, g) = \int_\Omega f(x)g(x)\,\mathrm{d}x$, and the mean of scalar series h_n as $\langle h_n\rangle \equiv \frac{1}{N}\sum_{n=1}^{N} h_n$.

If φ is defined as a linear combination of the snapshots v_n:

$$\varphi(x) = \sum_k a_k v_k(x) \tag{2}$$

the objective of maximizing λ can be transformed into an eigenvalue problem:

$$C_{nk}a_k = \lambda a_n \tag{3}$$

where

$$C_{nk} \equiv \frac{1}{N}(v_n, v_k). \tag{4}$$

Since C_{nk} is symmetric and positive definite, the eigenvectors of equation (3) can be substituted into equation (2) to yield eigenfunctions (basis functions) $\varphi(x)$. The eigenfunction corresponding to the largest eigenvalue is the most representative shape of fields extracted from the ensemble of the snapshots v_n, the eigenfunction corresponding to the second largest eigenvalue is the second most representative shape of fields, and so on [11]. In practice, the snapshots can be obtained from a few transient coupled-domain FEM/FDM simulation runs.

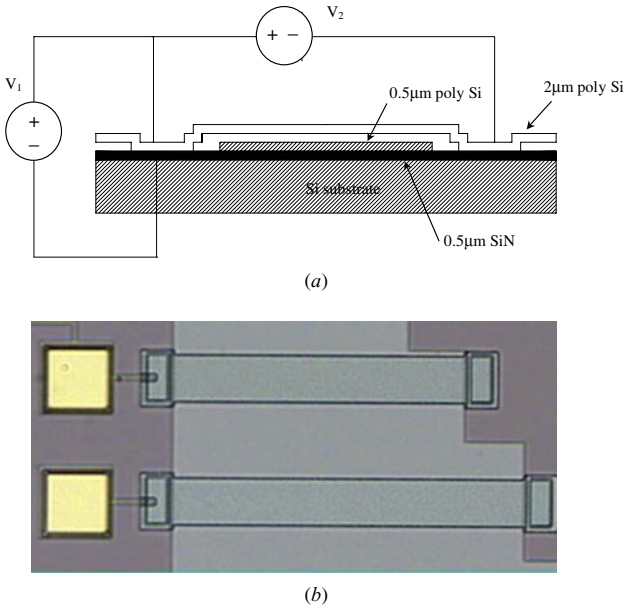

(*a*)

(*b*)

Figure 1. (*a*) A schematic of the device analysed in this work. (*b*) A CCD picture (top view) of two micro fixed–fixed beams studied in this work.

3. Macromodeling of coupled-domain systems

In this section, a MEMS case study example, as well as two macromodeling techniques, the Arnoldi method and the Galerkin method, will be presented. The MEMS example studied in this work is a fixed–fixed-beam structure fabricated by the MUMPs® process [12], as shown in figure 1. The electrostatic force distribution caused by the voltage difference (V_1) between the beam and the bottom electrode actuates (pulls down) the beam. This mechanism is widely used in resonance- or switch-type devices. If another voltage source is connected between the two ends of the beam (V_2), an electric current flowing through the beam results in Joule heating. The temperature increase caused by the heating changes the internal stress of the beam structure, affecting the device dynamics.

The fixed–fixed-beam system can be modeled by coupling the 1D beam equation for structural dynamics [13], the 2D Reynold's equation for squeeze-film damping [14] and the 3D heat transfer equation for thermal effect [15]. The electrostatic force is included in the beam equation as a distributed load using the analytical parallel-plate approximation. The governing equations are shown below:

$$EI\frac{\partial^4 d}{\partial x^4} - A(\sigma_r - (\alpha_0\Delta T - \varepsilon)E)\frac{\partial^2 d}{\partial x^2} = F_{\mathrm{elec}} + F_{\mathrm{air}} - \rho\frac{\partial^2 d}{\partial t^2} \tag{5}$$

$$\frac{\partial^2 T}{\partial x^2} + \frac{\partial^2 T}{\partial y^2} + \frac{\partial^2 T}{\partial z^2} + \frac{\dot{q}}{k} = \frac{\rho_{\mathrm{si}}C_P}{k}\frac{\partial T}{\partial t} \tag{6}$$

Table 1. The variables and properties of the governing equations.

l	Beam length
h	Beam thickness ($=2\ \mu$m)
w	Beam width ($=40\ \mu$m)
A	Beam cross-section area ($=hw$)
I	Moment of inertia of the beam cross-section ($=wh^3/12$)
D	Displacement of the beam
P	Pressure distribution inside the gap
T	Temperature distribution of the beam
Kn	Knudsen's number ($=\lambda/(d+d_0)$), where λ ($=0.064\ \mu$m) is the mean free path of air
E	Young's modulus of polysilicon ($=160$ Gpa)
ρ	Mass per unit length of the beam ($=h\cdot w\cdot 2330$ kg m^{-3})
ε_0	Free space permittivity
α_0	Coefficient of thermal expansion of polysilicon ($=2.6\times10^{-6}$/K)
ρ_{si}	Density of polysilicon ($=2330$ kg m^{-3})
C_P	Specific heat of polysilicon ($=920$ J kg^{-1} K)
k	Thermal conductivity of polysilicon ($=148$ W m^{-1} K) [20]
η	Air viscosity ($=1.82\times10^{-5}$ kg m s^{-1})
σ_r	Residual stress of the beam ($=-10$ MPa)
ε	Axial strain of the beam due to large deflection (stress stiffening effect)
ΔT	1D variation of temperature distribution along the x direction by averaging the temperature distribution in y and z directions
$\dot{q}$	Volume heat generation
F_{air}	Resistant force (N m)$^{-1}$ caused by the squeeze-film damping
F_{elec}	Electrostatic force (N m)$^{-1}$ using the parallel-plate approximation
d_0	Initial gap between the beam and the bottom electrode ($=2.0\ \mu$m)
P_0	Initial pressure inside the gap and the ambient pressure ($=1.013\times10^5$ N m^{-2})
T_0	Initial temperature of the structure and the ambient temperature ($=300$ K)

$$\nabla\cdot((1+6\mathrm{Kn})(d_0+d)^3p\nabla p)=12\eta\frac{\partial(p(d+d_0))}{\partial t} \tag{7}$$

$$F_{\mathrm{elec}}=\frac{-\varepsilon_0 wV^2}{2(d_0+d)^2} \tag{8}$$

$$F_{\mathrm{air}}=\int_0^w (p-p_0)\,\mathrm{d}y \tag{9}$$

$$\Delta T=\frac{\int_0^w\int_0^h (T-T_0)\,\mathrm{d}z\,\mathrm{d}y}{A}. \tag{10}$$

Table 1 lists the variables and the properties used in the governing equations. The beam is mechanically fixed at both ends, and the air pressure on both sides of the beam is fixed at ambient pressure p_0. The temperatures on the surfaces of both the beam's ends are fixed at 300 K, and the convection boundary condition is applied around all other surfaces of the beam. The governing equations listed above include a linear partial differential equation (the heat transfer equation) and two nonlinear partial differential equations (the beam equation and Reynold's equation). The macromodeling process, which will be described in the following subsections, employs the Arnoldi technique [3, 5, 16] to generate compact models for the linear equation. For the nonlinear equations, the K-L decomposition will be applied to extract basis functions, and the Galerkin method will be used to formulate reduced-order models [9, 10, 17].

3.1. Linear heat transfer macromodeling with Arnoldi-based algorithm

For the heat transfer effect, the beam is discretized using the finite difference scheme to represent the spatial derivatives of the heat transfer equation (equation (6)), which yields a set of ordinary differential equations:

$$\begin{aligned}\underline{\dot{x}}&=\underline{A}\underline{x}+\underline{B}\underline{u}\\ \underline{y}&=\underline{C}\underline{x}\end{aligned} \tag{11}$$

where $\underline{x}$ is the temperature distribution on each node, $\underline{A}$ is the system matrix (n by n) formulated by the finite-difference discretization (n is the total number of the nodes) and $\underline{u}$ is the scalar input function of the system. For this study, $\underline{u}$ is the prescribed volume heat generation function (in time), and the $\underline{B}$ matrix ($n\times1$) contains the corresponding scaling factors, which account for the distribution of the volume heat generation inside the beam. Finally, $\underline{C}$ is an $m\times n$ matrix and is deliberately formed so that the output vector y ($m\times1$) will be the 1D temperature distribution along the x direction, where m is the number of the beam discretizations in the x direction. In this work, $\underline{y}$ is identical to ΔT (equation (5)), and is the key variable for integrating the 3D heat transfer effect with the 1D beam equation for calculating the electro–thermal–mechanical effect.

Typically n is greater than 10 000 for the 3D thermal analysis, and thus significant computational resources are required for transient simulations. Therefore, the Arnoldi method [2, 3, 16] is applied to reduce the system matrices ($\underline{A}$, $\underline{B}$ and $\underline{C}$) into matrices with much lower orders ($\underline{A}_r$, $\underline{B}_r$ and $\underline{C}_r$). Then the thermal system can be represented as

$$\begin{aligned}\underline{\dot{x}}_r&=\underline{A}_r\underline{x}_r+\underline{B}_r\underline{u}\\ \underline{y}&=\underline{C}_r\underline{x}_r\end{aligned} \tag{12}$$

where

$$\begin{aligned}\underline{A}_r&=\underline{V}^T\underline{A}\underline{V}\qquad \underline{B}_r=\underline{V}^T\underline{B}\\ \underline{C}_r&=\underline{V}^T\underline{C}\end{aligned} \tag{13}$$

where $\underline{V}$ is the first q orthogonal bases $\{\vec{v}_i\}$ that spans the Krylov subspace:

$$K_q(\underline{A}^{-1}, \underline{b}) = \text{span}\{\underline{b}, \underline{A}^{-1}\underline{b}, \underline{A}^{-2}\underline{b}, \ldots, \underline{A}^{-(q-1)}\underline{b}\} \quad (14)$$

where $\underline{b} = -\underline{A}^{-1}\underline{B}$.

Note that the procedure of generating the orthogonal bases $\{\vec{v}_i\}$ is in fact the Gram–Schmidt process with the initial bases $\{\underline{b}, \underline{A}^{-1}\underline{b}, \underline{A}^{-2}\underline{b}, \ldots, \underline{A}^{-(q-1)}\underline{b}\}$. This procedure of generating macromodels has been implemented as an automatic process in this work. Since most MEMS thermal devices are operated below 10 MHz, the typical required order q of the reduced system (equation (12)) is less than 30 [5], which makes the computations of transient and frequency responses extremely efficient. In other words, the reduced system still provides the results of interest (the output $\underline{y}$) based on the prescribed variables (input $\underline{u}$), but requires much less state variables ($\underline{x}_r$) than the original system.

It has to be emphasized that one of the performance bottlenecks of creating compact models using the Arnoldi-based method is the number of the independent sources in the input vector $\underline{u}$. The longer the $\underline{u}$ vector, the larger the required Krylov subspace due to a bigger $\underline{B}$ matrix, which in turn increases the cost of generating reduced-order models [18]. This bottleneck happens quite frequently as the algorithm is used for macromodeling integrated circuits (IC) with hundreds or thousands of independent sources. Fortunately, for most MEMS thermal systems, the number of independent input sources is usually quite small (less than 10). For our case, only one independent source exists in the thermal system. Therefore, in terms of macromodel generation efficiency, the Arnoldi-based method is also quite suitable for the thermal system studied in this work.

3.2. Nonlinear structure and damping macromodeling with Galerkin method

For the beam equation and Reynold's equation, we approximate the displacement and the pressure distribution as the superposition of the displacement basis functions D_i and the pressure basis function P_i obtained by the K-L decomposition technique:

$$\hat{d}(x, t) = d_0 + \sum_{i=1}^{M} \alpha_i(t) D_i(x) \quad (15)$$

$$\hat{p}(x, y, t) = p_0 + \sum_{i=1}^{N} \beta_i(t) P_i(x, y) \quad (16)$$

where M and N are the numbers of selected basis functions of displacement and pressure, respectively; $\alpha_i(t)$ and $\beta_i(t)$ are the time-dependent coefficients of the corresponding basis functions. Assume either of the partial differential equations is written as the following form:

$$\mathbf{L}(\psi) = f \quad (17)$$

where $\mathbf{L}$ is a differential operator, and ψ is the solution of field of the partial differential equation. In our case, ψ is either d or p.

The Galerkin condition requires that

$$(B_i, \mathbf{L}(\hat{\psi}) - f) = 0 \quad (18)$$

where B_i is the basis functions (D_i or P_i). $\hat{\psi}$ is either $\hat{d}$ or $\hat{p}$, and is the approximation of the field solution ψ.

Finally, equation (18) yields two sets of ordinary differential equations (i.e., the macromodels) that are reduced from the two original partial differential equations:

$$\mathbf{M}\ddot{\beta} + \mathbf{K}\beta + f = 0 \quad (19)$$

$$\mathbf{R}\dot{\alpha} + \mathbf{S}\alpha + r = 0 \quad (20)$$

where $\mathbf{M}_{ij} = \int_L \rho D_i D_j \, \mathrm{d}x$

$$\mathbf{K}_{ij} = \int_L \left(EI \frac{\partial^2 D_i}{\partial x^2} \frac{\partial^2 D_j}{\partial x^2} + A(\sigma_r - E(\alpha_0 \Delta T - \varepsilon)) \times \frac{\partial D_i}{\partial x} \frac{\partial D_j}{\partial x} \right) \mathrm{d}x$$

$$f_i = -\int_L D_i (F_{\text{elec}} + F_{\text{air}}) \, \mathrm{d}x$$

$$\mathbf{R}_{ij} = \int_S 12\eta \hat{d} P_i P_j \, \mathrm{d}x \, \mathrm{d}y$$

$$\mathbf{S}_{ij} = \int_S \left((1 + 6Kn)\hat{d}^3 \hat{p} \left(\frac{\partial P_i}{\partial x} \frac{\partial P_j}{\partial x} + \frac{\partial P_i}{\partial y} \frac{\partial P_j}{\partial y} \right) + 12\eta P_i P_j \frac{\partial \hat{d}}{\partial t} \right) \mathrm{d}x \, \mathrm{d}y$$

$$r_i = \int_S 12\eta p_0 P_i \frac{\partial \hat{d}}{\partial t} \, \mathrm{d}x \, \mathrm{d}y.$$

Since maximizing λ is equivalent to maximizing the mean '*energy*' (see equation (1)) of the snapshots v_n projected on the corresponding basis function φ (either D_i or P_i in this subsection), typically only the first few terms of the basis functions are required for equations (15) and (16) to account for most '*energy*' (characteristics) provided by the ensemble of snapshots. Consequently, the total required order ($= 2M + N$) of the macromodels for providing excellent approximation of the coupled-domain system is much less than the order of the fully-meshed coupled-domain FEM/FDM model, and thus the computational cost of the macromodel is much less than that of the FEM/FDM solvers.

4. Results and discussions

4.1. Accuracy and efficiency of macromodels

Using the finite-difference method, the fixed–fixed beam is meshed using a 1D grid (41 × 1 nodes) for the beam equation, a 2D grid (41 × 20 nodes) for the Reynold's equation and a 3D grid (41 × 20 × 3 nodes) for the heat transfer equation. The transient simulation of the fully-meshed FDM (*full-FDM*) model can be readily performed by using the Runge–Kutta method with adaptive time-step control [19]. However, the computational cost is quite expensive due to a large number of nodes. Extracting the basis functions using the K-L decomposition technique is even more expensive because it requires *a few* runs of transient full-FDM simulations for collecting snapshots of physical field distributions. Fortunately, the heat-transfer effect is weakly

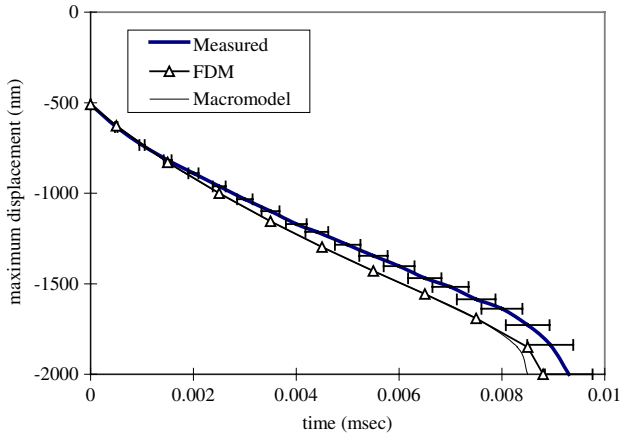

Figure 2. The measured and simulated pull-in dynamics of a 350 μm beam with an applied electrostatic voltage of 30 V. The simulated and measured results are the transient responses for the beam that is originally steadily balanced with the applied voltage of 7.8 V, which causes an initial deflection 509 nm.

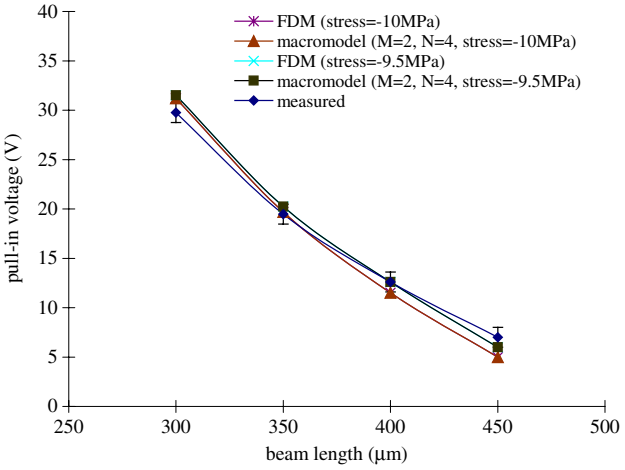

Figure 3. The measured and calculated pull-in voltages for beams with different lengths.

coupled with the 1D beam equation (i.e., we assume that the deformed shape of the beam will not affect the temperature distribution that is computed by assuming no deformation), and therefore, for extracting the displacement and the pressure basis functions, we set up a coupled-domain '*partial-FDM*' model, which computes the beam equation and the Reynold's equation using the finite-difference method, while calculating the heat transfer effect using the macromodel generated by the Arnoldi method. Using the partial-FDM model, the basis functions are created from an ensemble of four different step-input voltages for electrostatic actuation. For example, for a beam of 350 μm in length, four step-input electrostatic voltages of 21 V, 22 V, 25 V and 30 V are used. The voltage for electrothermal effect is fixed at 0.5 V, and the order (q) of the thermal macromodel is 5.

The measured and simulated pull-in dynamics of this 350 μm beam are shown in figure 2. Note that the two displacement basis functions and four pressure basis functions are used for the macromodels, and the electrothermal effect is not included. The measured transient response is obtained by an optical interferometer. In order to properly measure the transient, a TTL (digital) step signal is used to trigger the interferometer as well as to activate the applied voltage of 30 V by using a high-speed BJT switch. Because of the trigger circuitry, an initial dc voltage of 7.8 V between the beam structure and the substrate exists prior to the actuation of the applied voltage of 30 V. Therefore, the simulated and measured results are in fact the transient responses for the beam that is originally stably balanced with an applied voltage of 7.8 V, and then is actuated with 30 V. According to simulation, this initial voltage of 7.8 V results in a 509 nm displacement at the center of the beam. The figure shows that, after the actuation voltage of 30 V is applied, the macromodel follows the FDM model very well (less than 1% error) until pull-in occurs. Also, the simulated and measured results match each other pretty well during the early stage of the actuation, but deviate slightly after the beam travels about one-third of the initial gap. The measured and calculated pull-in voltages for the beams with different lengths are presented in figure 3. Note that the polysilicon residual stress provided by the foundry is –10 MPa. However, for the 400 μm-long and the 450 μm-long beams, the simulated results with residual stress of –9.5 MPa match the measured results better. Note that the simulated results with residual stresses from -9.3 MPa to -11.2 MPa will fall into the confidence limits (upper and lower) of the measured results (95% confidence interval).

Table 2 shows the comparison of the errors, the computational times and the speed-up factors for the full-FDM model, the partial-FDM model and the macromodels with different orders. These results are obtained by simulating the transient pull-in dynamics for a 350 μm beam using a PC with Pentium-III 1G CPU running the Linux operating system. The code is implemented in C-language. Compared with the full-FDM model, the partial-FDM model shows a significant reduction in computational time (about 2 orders of magnitude) with a very small discrepancy (less than 0.1%). This result indicates that the heat transfer model can be accurately modeled using macromodels with very low orders. It also implies that if three or more energy domains are

Table 2. A comparison of the average error, the computation time and the speed-up factor between the full-FDM model, the partial-FDM model and the macromodels.

Models	Number of ODEs	Average error	Computation time (s)	Speed-up factor
Full-FDM model	3362	N/A	8535	1.0
Partial-FDM (thermal: $q = 5$)	907	$\ll$0.1%	148	57.7
Macromodel ($M = 2, N = 4, q = 5$)	13	0.9%	17	502.1
Macromodel ($M = 2, N = 3, q = 5$)	12	0.9%	9	948.3
Macromodel ($M = 2, N = 2, q = 5$)	11	5.5%	4	2133.8

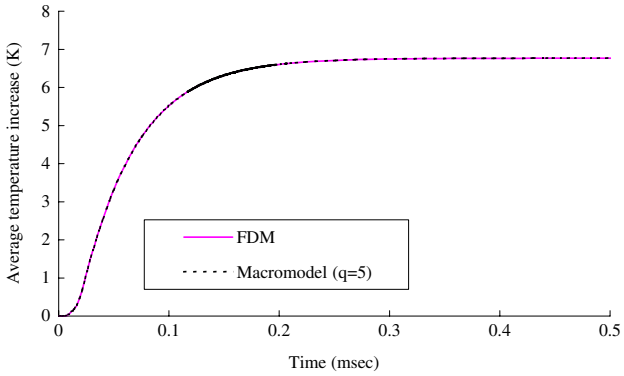

Figure 4. The transient response of the maximum temperature increases for a 250 μm-long beam. The applied heating voltage is 0.5 V.

simultaneously simulated using the FDM technique, the cost increases tremendously for extracting basis functions using the K-L decomposition.

4.2. Electro-thermal-mechanical effect

With an electrothermal voltage of 0.5 V, the transient average temperatures of a 250 μm-long beam calculated by the macromodel and the full-FDM model are shown in figure 4. As expected, the average temperature approaches a steady value when the heat-generation rate and the heat-dissipation rate balance each other. Note that the relative error of the maximum temperatures between the macromodel and the FDM model is less than 0.5%, which is indistinguishable in the figure. Also note that our preliminary study shows that, for the beam under a step heating voltage, the error can be confined within 1% if the order of the thermal macromodel is larger than 3 (i.e. $q > 3$).

The measured and simulated transient behavior of the beam with/without electrothermal effect is shown in figure 5. Obviously the *mechanical time constant*, which we define as one quarter of the inverse of the beam's damped frequency ω_d, is much shorter (at least 1 order of magnitude) than the thermal heating time constant indicated in figure 4. This phenomenon can also be observed by the dimensional analysis for the mechanical and thermal time constants of the beams. For a rule-of-thumb analysis, the damped frequency of the beam can be approximated as [21]:

$$\omega_d \propto \omega_n = (\beta L)^2 \sqrt{\frac{EI}{\rho A L^4}} \propto \sqrt{\frac{Ewh^3}{\rho whL^4}} \propto \frac{h}{L^2} \qquad (21)$$

where ω_d is the undamped resonance frequency, and βL is a tabulated constant that is close to 5, and can be found in typical vibration textbooks. For the beams studied in this work, the beam thickness h is a *fixed* parameter. Therefore, the relationship between the *mechanical time constant* τ_M and the beam dimensions is

$$\tau_M \propto L^2. \qquad (22)$$

Furthermore, using the lumped-element thermal parameters for the beam whose both ends are fixed at ambient temperature, the thermal time constant can be written as [15]

$$\tau_T = R_T C_T \qquad (23)$$

where $R_T (\propto L/A)$ is the effective lumped thermal resistance, and $C_T (\propto LA)$ is the effective lumped thermal capacitance.

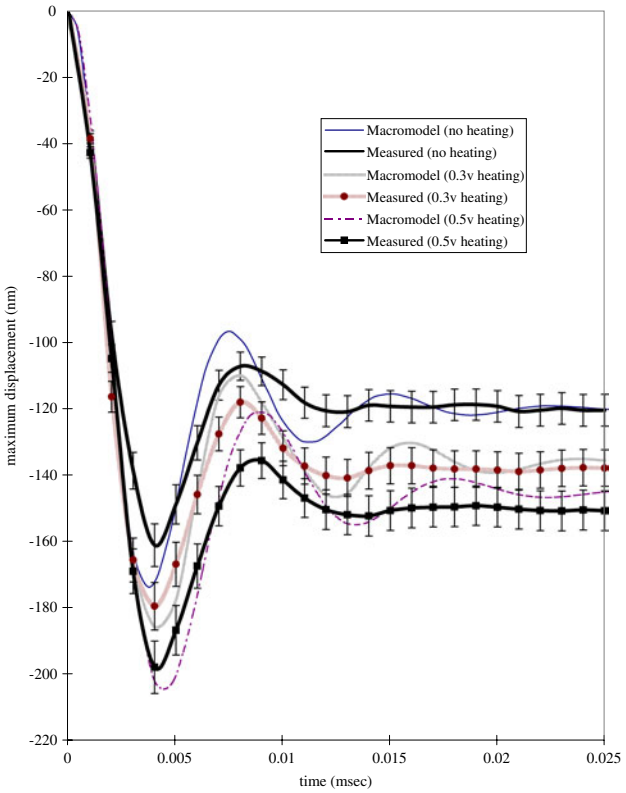

Figure 5. The transient behavior of a 250 μm-long beam with and without electrothermal effect. The applied step voltage for electrostatic actuation is 20 V.

Therefore, the relationship between the thermal time constant and its dimensions can also be approximated as

$$\tau_T \propto L^2. \qquad (24)$$

Hence, we may conclude that both the mechanical and thermal time constants are proportional to the square of the beam length, and are insensitive to (independent of) the beam width. The above analysis shows that no matter how we vary the dimensions of the beams (i.e., by changing the beam length or width), it is not possible to find a beam whose mechanical time constant is large enough to match the order of magnitude of its thermal time constant. Therefore, experimentally observing the coupled behavior due to the electrostatic and the electrothermal effects *on the same time scale* will not be feasible or necessary. Alternatively, we set up an experiment to observe the transient behavior of the beam under a thermally induced internal stress caused by preheating the beam electrothermally. Under a step electrostatic actuation voltage of 20 V, the transient behavior of a 250 μm beam with and without electrothermal effect is presented in figure 5. Note that, for the simulated case without electrothermal effect, the Young's modulus of the beam is adjusted by about 2% in order to match the steady-state displacement with that of the measured result. Using the same material properties, the simulated result with electrothermal effect also corresponds well to the measured result. The simulated results with Young's modulus from 155 GPa to 164 GPa will fall into the confidence limits (upper and lower) of the measured steady state displacements (95% confidence interval). Note that the simulated results underestimate the air damping effect. We

speculate that the discrepancy is due to the structural damping effect as well as the energy loss through the anchors. Also note that in this case the BJT switch is not used because the 20 V electrostatic voltage can be provided by a typical function generator. Therefore, the inherent 7.8 V, which has to be considered in figure 2, does not exist in figure 5.

5. Conclusion

This paper presented an approach for simulating complicated coupled-domain microsystems with electrostatic and electrothermal effects using model order reduction techniques. For nonlinear domains, the Karhunen-Loeve decomposition technique is used for extracting basis functions that will be then plugged into the reduced-order model formulated by the Galerkin method. For linear domains, the Arnoldi-based technique is used for generating compact models. The fundamental backgrounds of the techniques are described briefly. Fixed–fixed-beam microsystems, which include the structural dynamics, the squeeze-film damping, the heat transfer and the electrostatics domains, are modeled using this approach. The simulated results not only indicate that the system dynamic behavior can be accurately reproduced using the macromodels, but also demonstrate that this macromodeling approach reduces the computational cost by about 2–3 orders of magnitude. Using the full-FDM model, the computational cost increases significantly as the thermal effect is added into the system, which makes the Karhunen-Loeve method inefficient for extracting the basis functions. This bottleneck can be resolved by using a partial-FDM model, which is a combination of the coupled beam-damping-electrostatic FDM model and the thermal macromodel generated by the Arnoldi method. Analytical and simulated results also indicate that the thermal time constants are at least one order of magnitude larger than the mechanical time constants for the fixed–fixed beams studied in this work. Modeled pull-in and transient behavior of the beams is also verified with the measured results.

Acknowledgments

This work is partially supported by the NSC (National Science Council, Taiwan, ROC) through the grant contract no NSC-90-2218-E-002-031. The authors wish to thank C-C Yu, P-C Yen and Dr J-Y Wu for valuable discussions.

References

[1] Senturia S D 2001 *Microsystem Design* (Dordrecht: Kluwer)

[2] Wang F and White J 1998 Automatic model order reduction of a microdevice using the Arnoldi approach *ASME IMECE'98* DSC vol 66 pp 527–30

[3] Yang Y-J *et al* 2001 Modeling gas damping and spring phenomena in MEMS with frequency dependent macro-models *Proc. of IEEE MEMS 2001* pp 365–8

[4] Chen Y and White J 2000 A quadratic method for nonlinear model order reduction *Proc. Modeling and Simulation of Microsystems* pp 477–80

[5] Yang Y-J and Yu C-C 2004 Extraction of heat-transfer macromodels for MEMS devices *J. Micromech. Microeng.* **14** 587–96

[6] Rewienski M and White J 2001 A trajectory piecewise-linear approach to model order reduction and fast simulation of nonlinear circuit and micromachined devices *Proc. Computer-Aided Design* pp 252–7

[7] Rewienski M and White J 2002 Improving trajectory piecewise-linear approach to nonlinear model order reduction for micromachined devices using an aggregated projection basis *Proc. Modeling and Simulation of Microsystems (San Juan, Puerto Rico)* pp 128–31

[8] Hung E, Yang Y-J and Senturia S D 1997 Low-order models for fast dynamical simulation of MEMS microstructures *Proc. Transducers'97 (Chicago, June 1997)* pp 1101–4

[9] Hung E and Senturia S D 1999 Generating efficient dynamical models for microelectromechanical systems from a few finite-element simulation runs *J. Microelectromech. Syst.* **8**

[10] Park H M and Lee M W 1998 An efficient method of solving the Navier–Stokes equations for flow control *Int. J. Numer. Methods Eng.* **41** 1133–51

[11] Golub G H and Van Loan C F 1996 *Matrix Computations* (Baltimore MD: The John Hopkins University Press)

[12] MEMSCAP 2002 *MUMPS Design Handbook*, (MEMSCAP, Inc.)

[13] Timoshenko S P and Woinowsky-Krieger S 1959 *Theory of Plates and Shells* (New York: McGraw-Hill)

[14] Yang Y-J and Senturia S D 1996 Numerical simulation of compressible squeezed-film damping *Solid-State Sensor and Actuator Workshop, (Hilton Head, SC, June 1996)*

[15] Mills A F 1992 *Heat Transfer* (Boston: Richard D Irwin Inc.)

[16] Odabasioglu A, Celik M and Pileggi L T 1998 PRIMA: passive reduced-order interconnect macromodeling algorithm *IEEE Trans. Comput.-Aided Des. Integr. Circuits Sys.* **17** 645–54

[17] Chen J and Kang S 2000 An algorithm for automatic model-order reduction of nonlinear MEMS devices *Proc. IEEE Int. Symp. Circuits and Systems (Geneva, Switzerland, May, 2000)* pp 445–8

[18] Wang J M and Nguyen T V 2000 Extended krylov subspace method for reduced order analysis of linear circuits with multiple sources *Proc. 37th Design Automation Conference (DAC 2000) (Los Angeles, CA, June, 2000)* pp 247–52

[19] Press W H, Flannery B P, Teukolsky S A and Vetterling W T 1993 *Numerical Recipes in C: The Art of Scientific Computing* 2nd ed (Cambridge: Cambridge University Press)

[20] Lide D R and Kehiaian H V (eds) 1994 *CRC Handbook of Thermophysical and Thermomechanical Data* (Boca Raton, FL: CRC Press)

[21] Rao S S 1990 *Mechanical Vibrations* (Reading, MA: Addison-Wesley)